metals

MDPI

Article

Change in Superparamagnetic State Induced by Swift Heavy Ion Irradiation in Nano-Maghemite

Sándor Stichleutner [1,*], Bence Herczeg [1], Jiří Pechoušek [2], Libor Machala [2], Zoltán Homonnay [1], David Smrčka [2], Lukáš Kouřil [2], René Vondrášek [2], Mátyás Kudor [1], Vladimir A. Skuratov [3,4,5], Luboš Krupa [2,3], Shiro Kubuki [6] and Ernő Kuzmann [1]

1 Institute of Chemistry, Eötvös Loránd University, Pázmány P. s. 1/A, 1117 Budapest, Hungary
2 Department of Experimental Physics, Faculty of Science, Palacký University Olomouc, 17. listopadu 1192/12, 77146 Olomouc, Czech Republic
3 Flerov Laboratory of Nuclear Reactions, Joint Institute for Nuclear Research, JINR, Joliot-Curie 6, 141980 Dubna, Russia
4 Department of Nuclear Physics, Dubna State University, Universitetskaya 19, 141980 Dubna, Russia
5 Institute of Nuclear Physics and Engineering, National Research Nuclear University MEPhI, Kashirskoye Sh. 31, 115409 Moscow, Russia
6 Department of Chemistry, Graduate School of Science and Engineering, Tokyo Metropolitan University, 1-1, Minami-Osawa, Hachi-Oji, Tokyo 192-0397, Japan
* Correspondence: stichleutner@izotop.hu

Abstract: The effect of swift heavy ion irradiation on sol–gel-prepared maghemite nanoparticles was studied by ^{57}Fe transmission Mössbauer spectroscopy and X-ray diffractometry (XRD). The room temperature Mössbauer spectra of the non-irradiated nano-maghemite showed poorly resolved magnetically split, typical relaxation spectra due to the superparamagnetic state of the nanoparticles. Significant changes in the line shape, indicating changes in the superparamagnetic state, were found in the Mössbauer spectra upon irradiation by 160 MeV and 155 MeV $^{132}Xe^{26+}$ ions with fluences of 5×10^{13} ion cm^{-2} and 1×10^{14} ion cm^{-2}. XRD of the irradiated maghemite nanoparticles showed a significant broadening of the corresponding lines, indicating a decrease in the crystallite size, compared to those of the non-irradiated ones. The results are discussed in terms of the defects induced by irradiation and the corresponding changes related to the change in particle size and consequently in the superparamagnetic state caused by irradiation.

Keywords: nano-maghemite; Mössbauer spectroscopy; swift heavy ions; superparamagnetism; radiation effects

check for updates

Citation: Stichleutner, S.; Herczeg, B.; Pechoušek, J.; Machala, L.; Homonnay, Z.; Smrčka, D.; Kouřil, L.; Vondrášek, R.; Kudor, M.; Skuratov, V.A.; et al. Change in Superparamagnetic State Induced by Swift Heavy Ion Irradiation in Nano-Maghemite. *Metals* **2024**, *14*, 421. https://doi.org/10.3390/met14040421

Academic Editor: Aphrodite Ktena

Received: 25 February 2024
Revised: 24 March 2024
Accepted: 31 March 2024
Published: 3 April 2024

Copyright: © 2024 by the authors. Licensee MDPI, Basel, Switzerland. This article is an open access article distributed under the terms and conditions of the Creative Commons Attribution (CC BY) license (https://creativecommons.org/licenses/by/4.0/).

1. Introduction

Metal and metal oxide nanoparticles can be widely used in magnetic fluids, data storage, catalysis and biomedical applications such as magnetic bio-separation, hyperthermia, biological detection, detoxification, medical diagnosis, immunoassays, tissue repair, tumor therapy, targeted drug delivery, etc. [1–7]. Superparamagnetic iron oxide nanoparticles (SPIONs), thanks to their superparamagnetic properties, have found applications, among others, in environmental remediation and in cancer nanotheranostics, and they are very promising in oncological therapy (especially in the brain, breast, prostate and pancreatic tumors) [8–16].

Production and handling parameters can greatly influence properties that are important for use of nanomaterials. One treatment option for modifying nanomaterials is by irradiation with high-energy heavy ions. In doing so, a large amount of crystal defects can be introduced into these nano-systems upon irradiation.

In the case of metal-nanoparticles, a number of works [17–35] revealed that swift heavy ion irradiation induced shape deformations. A spherical to rod-like shape transformation occurs with the direction of nanoparticle elongation aligned to that of the incident ion,

while small nanoparticles below a critical diameter do not elongate, but dissolve in the matrix. The three-dimensional computation of the thermal spike model was applied for the explanation of the effect of swift heavy ion irradiation. A rational description of the ion-beam-shaping process for all nanoparticle dimensions as a function of the irradiation parameters was presented. The existence of both threshold and saturation fluences for the elongation effects and their dependence on ion energy and initial nanoparticle size was also established. Modification and controlled shaping of nanostructures by different energy ion beam irradiations were investigated and suggested.

Swift heavy ion irradiation-induced modifications in structural, magnetic and electrical transport properties of metal oxides were also experienced [36–45]. In the case of nano-iron oxides, phase transformation (e.g., magnetite to maghemite) and changes in transition temperatures (Verwey-temperature), as well as changes in magnetic anisotropy were observed. The overlap of swift heavy ion tracks, dislocation loop formation, oxygen diffusion and oxide phase formation by swift heavy ion irradiation were considered for the explanation of the findings.

Mössbauer spectroscopy is a unique method to study iron-oxide nanoparticles [46–48], especially to monitor their superparamagnetic states. Recently, we successfully applied Mössbauer spectroscopy to observe the formation of swift heavy ion irradiation-induced amorphous iron and superparamagnetic Fe–Si oxide phases [49], as well as change in magnetic anisotropy of nanostructured FINEMET alloys [50].

The main goal of our study was to investigate the effect of swift heavy ion irradiation on the iron microenvironments of nano-maghemites. For the characterization of non-irradiated and irradiated samples ^{57}Fe Mössbauer spectroscopy and XRD measurements were used.

2. Materials and Methods

The initial nano-Fe_3O_4 sample was prepared according to work [51]. Mohr's salt (2.627 g) was added to $(NH_4)_3Fe(C_2O_4)_3 \cdot 3H_2O$ (5.693 g) and dissolved in 250 mL of deionized water. After maintaining the reaction temperature at 30 °C, an additional 1.5 g of $NaNO_3$ and 50 mL of 25% aqueous NH_3 were poured into the aqueous solution and stirred for 15 min. Finally, the precipitate was washed with distilled water and ethanol and dried for half a day. From a portion of the resulting nano-magnetite product, nano-maghemite (nano-γ-Fe_2O_3) was prepared by heat treatment at 250 °C for 30 min in an air atmosphere [51].

Swift heavy ion irradiation of nano-maghemite was carried out with $^{132}Xe^{26+}$ ions of 160 MeV energy with a fluence of 5×10^{13} ion cm^{-2} and of 155 MeV energy with a fluence of 1×10^{14} ion cm^{-2} at room temperature, at a current density of 0.01 μA cm^{-2} and at a pressure of about 10^{-3} Pa, at the IC-100 cyclotron of the Flerov Laboratory of Nuclear Reactions, JINR, Dubna, Russian Federation between 2020 and 2021. The irradiation energies and fluences were chosen according to the values at which radiation effects have already been observed in related systems [49,50] and which were actually available at the facility. The plane of the samples was oriented perpendicular to the ion beam direction. Uniform ion distribution (to within 10%) over the irradiated sample surface was achieved by scanning in the horizontal and vertical directions. The temperature of target backing was controlled during the irradiation.

The irradiations were performed on powdered samples. Samples were prepared by evenly distributing powders on 5 μm thick Al foils. Samples were also prepared on a 2 mm thick 15 mm diameter Al foil by a suitably weighed amount of material (4 mg), in which case the original powders were fixed on the Al foils with different gluing. The maghemite powder was fixed to the Al foil using either Ag conducting paint or mixed solution (titrated to pH = 7) of polyethyleneimine (PEI) and NaCl adhesive.

^{57}Fe Mössbauer spectroscopy measurements of non-irradiated and irradiated samples were performed at room temperature (295 K) and at 80 K in transmission geometry. Conventional Mössbauer spectrometers (WISSEL type) were applied in constant acceleration

mode with integrated multichannel analyzers, collecting counts in 512 channels. At 80 K, the Mössbauer spectra were recorded by means of a JANIS liquid helium cryostat using a separate WISSEL spectrometer. The Mössbauer spectra were measured by a scintillation detector using a ^{57}Co(Rh) source with an activity of 1.8 GBq. The direction of the γ-rays was perpendicular to the plane of samples in all cases of Mössbauer measurements. Isomer shifts were given relative to α-iron. The evaluation of Mössbauer spectra was performed by least-square fitting of the lines using the MOSSWINN code [52].

Powder X-ray diffractograms of the samples were recorded by a computer-controlled DRON-2 X-ray diffractometer. The diffractograms were measured using $Fe_{K\alpha}$ radiation (λ = 0.179026 nm) and β filter, at tube generation of 45 kV and 35 mA, at room temperature in Bragg–Brentano geometry in the range of 2Θ = 20–90° with a goniometer speed of 0.25° min^{-1}. The computer evaluation of the XRD patterns was made by the EXRAY code. For phase identification the PCPDF Diffraction Data were used.

3. Results and Discussion

The room temperature (RT) Mössbauer spectra of the nano-maghemite samples, non-irradiated and irradiated with 160 MeV and 155 MeV energy Xe ions with fluences of 5×10^{13} ion cm^{-2} and 1×10^{14} ion cm^{-2}, respectively, are shown in Figure 1.

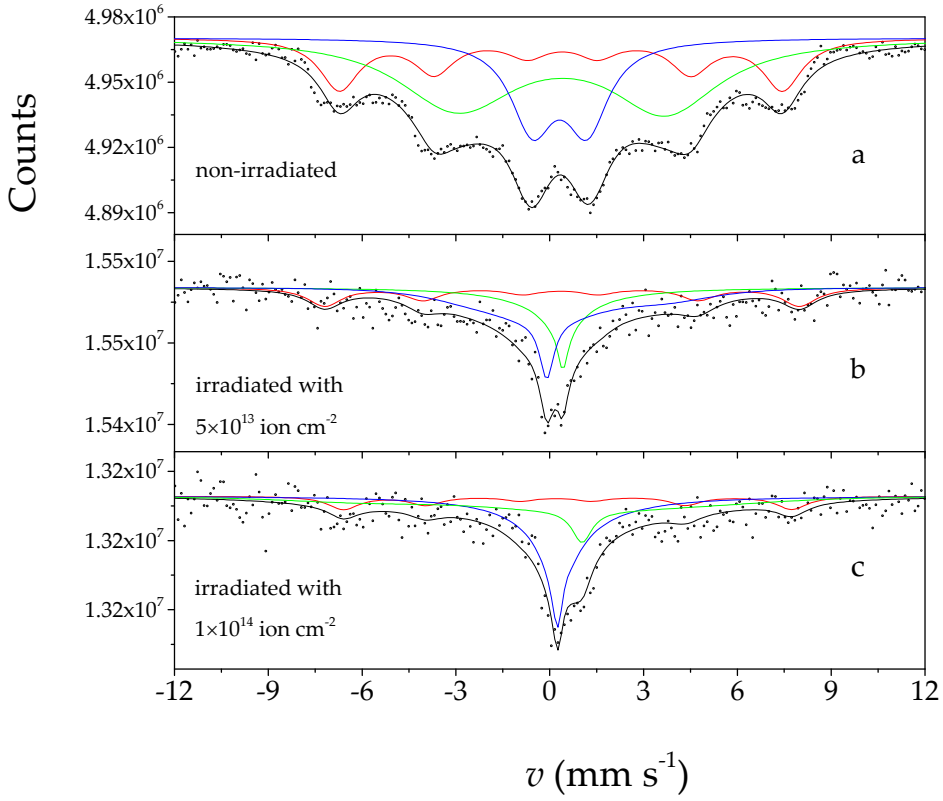


Figure 1. Room temperature Mössbauer spectra of nano-maghemite samples before irradiation (**a**), irradiated with 160 MeV Xe ions with a fluence of 5×10^{13} ion cm^{-2} (**b**) and irradiated with 155 MeV Xe ions with a fluence of 1×10^{14} ion cm^{-2} (**c**).

The RT Mössbauer spectrum of the non-irradiated sample (Figure 1a) shows a poorly resolved magnetic splitting. The spectrum fully corresponds to the nano-maghemite sample in the previous work [51]. This spectrum is characteristic to the RT spectrum of a nano-iron oxide in a superparamagnetic state [53]. This is because nano-iron oxides, depending on their particle size (generally, roughly below 15 nm), at RT show a spectrum with paramagnetic or poorly resolved magnetic splitting well below their magnetic ordering temperature (Neel or Curie temperature), while the Mössbauer spectrum of the bulk particle size oxide is the given magnetically split spectrum [54] with parameters diagnostically characteristic

of the oxide. This can be well explained by the superparamagnetic property related to the grain size, which is well reflected in the Mössbauer spectra. Superparamagnetic phenomenon can be observed with small ferromagnetic and antiferromagnetic grains behaving like huge paramagnetic particles. The grain size (or particle size) influences the relaxation time, τ, of the paramagnetic spin fluctuation as follows [55,56]:

$$\tau = \tau_0 e^{\frac{KV}{kT}} \quad (1)$$

where K is the anisotropy constant, V is the particle (grain) volume, k is Boltzmann constant and T is the absolute temperature.

The hyperfine splitting can appear in the Mössbauer spectrum if the paramagnetic spin relaxation is relatively slow, the relaxation time, τ, is much higher compared to the time of the Larmour precession ($2\pi/\omega_L$), where ω_L is the Larmour frequency ($\omega_L = \frac{g_I}{h} m_I \mu_N B$, where g_I is the gyromagnetic factor, m_I is the magnetic quantum number, μ_N is the nuclear magneton and B is the effective magnetic induction).

Since the relaxation time, τ, is the function of the temperature T, at a given temperature the relaxation time can be equal to the time of Larmour precession at the superparamagnetic transition characterized by τ_{sup} when the magnetic splitting collapses in the spectrum:

$$\tau_{sup} = \frac{2\pi}{\omega_L} \quad (2)$$

Consequently, on the basis of the temperature dependence of the Mössbauer spectra, it can be well determined when the nanostructured material is in the superparamagnetic state and when it is not. Furthermore, estimates can be made for the particle size and its distribution [57–59].

In accordance with the above, the non-irradiated nano-maghemite room temperature spectrum shown in Figure 1a could also be interpreted as a spectrum reflecting superparamagnetic relaxation. Since the Mössbauer spectra of nano-maghemite can be interpreted as a superposition of spectra reflecting three different Fe microenvironments [51,60], the RT spectrum of the non-irradiated sample was also decomposed into three subspectra. In the process, the magnetically poorly resolved subspectra were evaluated by fitting the Blume–Tjon relaxation model [52,56], from which we also obtained information on the relaxation frequencies. The model implemented in the Mosswinn code provided the jump rate, n, between two states of the fluctuating paramagnetic hyperfine field as a fitted parameter, which was related to the relaxation frequency, f, in the form of $n = lg2\pi f$. Then the relaxation time, τ, could be obtained as the reciprocal of the relaxation frequency. The fitting of the spectra was based on an arbitrarily chosen mathematical model, aiming to provide a guideline reflecting the changes induced by the irradiation in the superparamagnetic transition. The obtained Mössbauer parameters are shown in Table 1, which were the same as the values obtained in the previous work [51,60], where the relaxation related hyperfine parameters were restricted for the maghemite states studied in this work.

A large change could be observed in the RT Mössbauer spectra of the irradiated sample (Figure 1b) as a result of irradiation with 5×10^{13} ions cm^{-2} Xe ions compared to the spectrum of the non-irradiated sample (Figure 1a). The shape of the envelope of the Mössbauer spectrum of the irradiated nano-maghemite changed to a definite extent compared to the non-irradiated one, which could be clearly observed by the visual aspect, too. The Mössbauer spectrum of the irradiated sample was analyzed by the model taking into account the superparamagnetic relaxation, similarly to the non-irradiated one, and it was found that the spectrum of the irradiated sample could also be characterized by the relaxation frequencies. The parameters shown in Table 1 indicate that the corresponding relaxation frequencies increased in the irradiated sample, which could reflect that the irradiated sample was in a superparamagnetic state presented to a greater extent at RT than in the non-irradiated one.

Table 1. Room temperature Mössbauer parameters of nano-maghemite samples before and after irradiation with Xe ions with fluences of 5×10^{13} ions cm^{-2} and 1×10^{14} ions cm^{-2}.

Spectrum	T (K)	Component	Species	A (%)	δ (mm s^{-1})	Δ (mm s^{-1})	B_{int} (T)	$f = 10^{n-lg\pi}$ n
Non-irradiated maghemite	295	Sextet (1)	Fe^{3+}	26.1 (±1.1)	0.38 (±0.03)	−0.04 (±0.03)	44.1 (±0.4)	-
		Relaxation (1)	Fe^{3+}	49.8 (±1.8)	0.37 (±0.02)	0.25 (±0.03)	44.2 (±0.4)	7.11
		Relaxation (2)	Fe^{3+}	24.1 (±1.4)	0.32 (±0.03)	-	30.0 (±0.3)	7.58
Irradiated with Xe with 5×10^{13} ions cm^{-2}	295	Sextet (1)	Fe^{3+}	24.2 (±0.9)	0.37 (±0.03)	−0.2 (±0.03)	47.2 (±0.4)	-
		Relaxation (1)	Fe^{3+}	28.8 (±1.9)	0.35 (±0.03)	0.23 (±0.03)	45.0 (±0.4)	9.02
		Relaxation (2)	Fe^{3+}	46.5 (±1.7)	0.31 (±0.03)	-	23.0 (±0.3)	8.19
Irradiated with Xe with 1×10^{14} ions cm^{-2}	295	Sextet (1)	Fe^{3+}	15.9 (±1.3)	0.38 (±0.03)	−0.21 (±0.03)	38.5 (±0.4)	-
		Relaxation (1)	Fe^{3+}	48.2 (±1.9)	0.35 (±0.02)	0.26 (±0.03)	50.0 (±0.4)	9.12
		Relaxation (2)	Fe^{3+}	35.9 (±1.8)	0.32 (±0.03)	-	45.1 (±0.3)	8.42

A: relative spectral area, δ: isomer shift, Δ: quadrupole splitting, B: mean hyperfine magnetic field, f is the frequency of superparamagnetic relaxation.

In the case of the RT spectrum (Figure 1c) of the sample irradiated with Xe ions with the higher fluence (1×10^{14} ions cm^{-2}), the spectral envelope reflected even more paramagnetic contribution than observed with that of the sample irradiated with the lower fluence (Figure 1b). The increase in relaxation frequencies (Table 1) obtained with spectral evaluation supports that the irradiation with the higher fluence induced a more developed superparamagnetic state at room temperature in this sample.

Figure 2 shows the 80 K Mössbauer spectra of nano-maghemite samples, non-irradiated and irradiated with Xe ions with energies of 160 MeV and 155 MeV with fluences of 5×10^{13} ion cm^{-2} and 1×10^{14} ion cm^{-2}, respectively.

The Mössbauer spectrum of non-irradiated nano-maghemite measured at 80 K (Figure 2a) showed an envelope with a well-resolved magnetic splitting, in which no paramagnetic spectral contribution occurred. The spectrum could be decomposed into three sextets, which corresponded to the Fe^{3+} microenvironments found in nano-maghemite. The Mössbauer parameters obtained during the evaluation (Table 2) were the same as those reported in the previous work [51]. (We note here that the spectra shown in Figure 2 had a slight base line slope and curvature due to the cosine-effect related to the short distance between the source and detector. This could be completely eliminated during the evaluation, which was also indicated by the fact that the Mössbauer parameters were the same as the previously measured values.) The typical parameters of the well-resolved sextets (Table 2) and the absence of the paramagnetic component also indicated that the non-irradiated nano-maghemite sample at 80 K was no longer in a superparamagnetic state, but showed magnetic ordering.

Table 2. 80 K Mössbauer parameters of nano-maghemite samples before and after irradiation with Xe ions with fluences of 5×10^{13} ions cm^{-2} and 1×10^{14} ions cm^{-2}.

Spectrum	T (K)	Component	Species	A (%)	δ (mm s^{-1})	Δ (mm s^{-1})	B_{int} (T)	$f = 10^{n-lg\pi}$ n
Non-irradiated maghemite	80	Sextet (1)	Fe^{3+}	48.2 (±1.3)	0.46 (±0.02)	−0.02 (±0.03)	51.5 (±0.3)	-
		Sextet (2)	Fe^{3+}	35.8 (±1.1)	0.43 (±0.02)	0.01 (±0.03)	48.7 (±0.3)	-
		Sextet (3)	Fe^{3+}	16.0 (±0.8)	0.47 (±0.02)	0.04 (±0.04)	44.8 (±0.3)	-
Irradiated with Xe with 5×10^{13} ions cm^{-2}	80	Sextet (1)	Fe^{3+}	43.5 (±1.3)	0.46 (±0.02)	0.00 (±0.03)	51.6 (±0.3)	-
		Sextet (2)	Fe^{3+}	36.6 (±1.0)	0.44 (±0.02)	−0.02 (±0.03)	48.9 (±0.3)	-
		Sextet (3)	Fe^{3+}	19.9 (±1.0)	0.43 (±0.02)	−0.02 (±0.03)	45.3 (±0.3)	-
Irradiated with Xe with 1×10^{14} ions cm^{-2}	80	Sextet (1)	Fe^{3+}	41.1 (±1.5)	0.39 (±0.02)	−0.08 (±0.03)	48.5 (±0.3)	-
		Sextett (2)	Fe^{3+}	33.2 (±1.3)	0.46 (±0.02)	−0.07 (±0.03)	44.8 (±0.4)	-
		Sextett (3)	Fe^{3+}	6.4 (±1.6)	0.52 (±0.04)	0.20 (±0.05)	39.8 (±0.5)	-
		Relaxation *	Fe^{3+}	19.3 (±1.9)	0.52 (±0.04)	0.1 (±0.03)	55.0 (±0.4)	9.56

A: relative spectral area, *δ*: isomer shift, Δ: quadrupole splitting, *B*: mean hyperfine magnetic field, *f* is the frequency of superparamagnetic relaxation. * This paramagnetic component was evaluated as the result of the superparamagnetic relaxation by the help of the Blume–Tjon magnetic relaxation model.

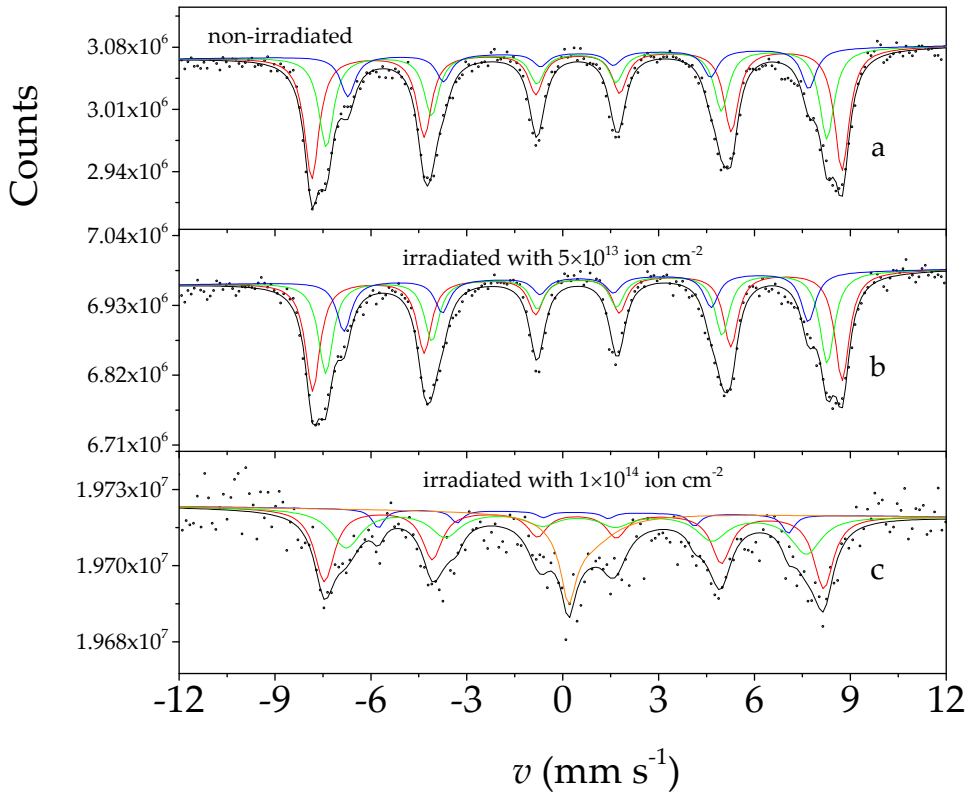


Figure 2. 80 K temperature Mössbauer spectra of nano-maghemite samples before irradiation (**a**) and irradiated with 160 MeV Xe ions with a fluence of 5×10^{13} ion cm^{-2} (**b**); irradiated with 155 MeV Xe ions with a fluence of 1×10^{14} ion cm^{-2} (**c**).

The 80 K Mössbauer spectrum of the nano-maghemite irradiated with a fluence of 5×10^{13} ions cm^{-2} (Figure 2b) was very similar to that of the non-irradiated sample (Figure 2a); the paramagnetic spectrum contribution did not appear here either. The parameters obtained by resolution into three sextets (Table 2) did not reflect a significant difference compared to the non-irradiated ones, despite the fact that the RT spectra were significantly different (Figure 1, Table 1). The result showed that at 80 K, the nano-maghemite sample irradiated with the lower fluence was in a magnetically ordered state.

In contrast to this, the 80 K Mössbauer spectrum of the nano-maghemite sample irradiated with a higher fluence of 1×10^{14} ions cm^{-2} (Figure 2c) revealed the appearance of a significant paramagnetic component in addition to the magnetically split spectrum contribution. This was evaluated for three sextets and one Blume–Tjon relaxation component, the results of which are shown in Table 2. The Mössbauer parameters obtained using such a model corresponded well to the fact that the higher fluence of irradiation induced the appearance of a superparamagnetic phase in the sample to an extent that a part of it (around 15%) was present in the superparamagnetic state even at 80 K. We note, however, that it could not be entirely ruled out that the paramagnetic component appearing in the higher fluence spectrum may have been related to a new paramagnetic phase created by the irradiation, different from maghemite. However, this was not supported by our measurements and the XRD did not indicate the formation of a new iron-bearing phase either.

Consequently, we assigned the observed Mössbauer results to changes in the superparamagnetic state induced by swift heavy ion irradiation in the nano-maghemite. The RT Mössbauer spectrum of the non-irradiated nano-maghemite showed poorly resolved magnetically split, typical relaxation spectra due to their superparamagnetic state of the nanoparticles. The significant changes in the line shape, found in the Mössbauer spectra of maghemite nanoparticles upon the irradiation by 160 MeV and 155 MeV $^{132}Xe^{26+}$ ions with fluences of 5×10^{13} ion cm^{-2} and 1×10^{14} ion cm^{-2}, respectively, reflected changes in the superparamagnetic relaxation state.

The XRD patterns of nano-maghemite samples, non-irradiated and irradiated with 155 MeV energy Xe ions with a fluence of 1×10^{14} ion cm^{-2} are shown in Figure 3.

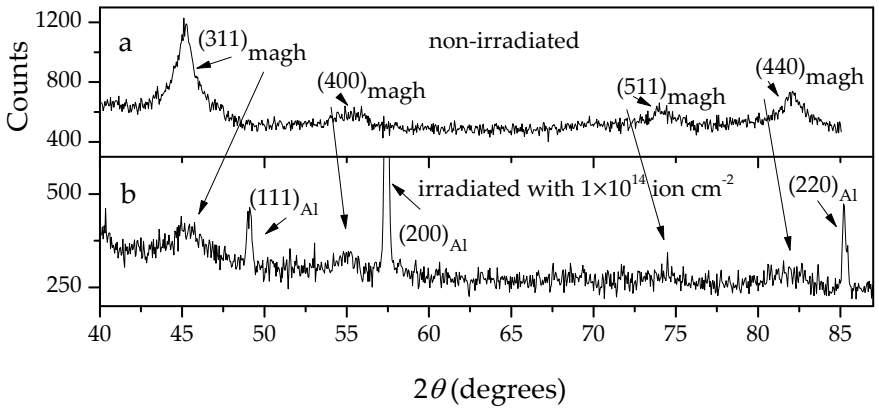


Figure 3. XRD patterns of nano-maghemite samples before irradiation (**a**) and irradiated with 155 MeV Xe ions with a fluence of 1×10^{14} ion cm^{-2} (**b**).

The XRD pattern of the non-irradiated sample (Figure 3a) showed an X-ray diffractogram with broad lines typical of nano-maghemite. The diffractogram fully corresponded to what was reported for the nano-maghemite sample in the previous work [51]. All the lines in the diffractogram of the non-irradiated sample matched well with those of the standard pattern of maghemite, PCPDFWIN card 39-1346 [61]. The lattice parameter was determined to be a = 0.83515 nm in agreement with the literature data.

The XRD diffractogram of the sample irradiated with 155 MeV Xe ions with a fluence of 1×10^{14} ion cm^{-2} (Figure 3b) was well evaluated to the broad line pattern of maghemite

and the sharp line pattern of Al. The presence of Al in the sample was attributed to the Al foil to which the powder was fixed with PEI glue. The relatively low occurrence of nano-maghemite could be explained by the very small amount of nano-maghemite used for the preparation of the irradiated sample satisfying the precondition that less than 8 µm thin layer of maghemite should be present on the Al surface to not exceed the penetration depth of the 155 MeV Xe ions. No new phase formation could be found in the irradiated samples by XRD analysis.

The crystallite sizes of the non-irradiated and irradiated nano-maghemites were determined from the corresponding X-ray diffractograms. The determination of crystallite size based on the Scherrer equation [62], $D = K\lambda/\beta\cos\theta$, was used to calculate the crystallite size of the nanoparticles, where D is the nanoparticle crystallite size, K represents the Scherrer constant (0.94), λ denotes the wavelength (0.179026 nm) and β denotes the full width at half maximum. After an optimized background subtraction, least-square fitting of the selected reflections of the diffractograms (Figure 4) was used for the more accurate determination of θ and β. The standard deviations of θ and β were determined by Monte Carlo error calculation, while the errors of D were derived based on the error propagation and taking into account three confidence intervals. The derived crystallite sizes D (together with their minimum and maximum values) are shown in Table 3.

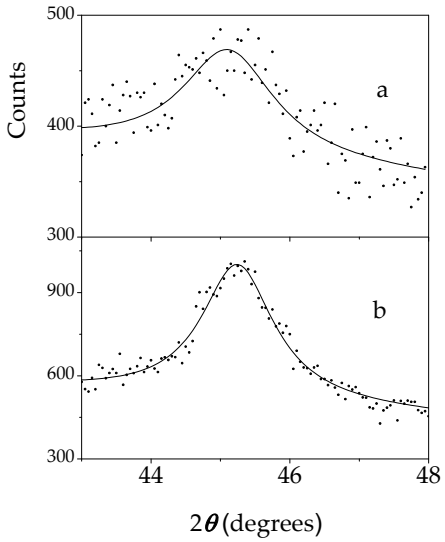


Figure 4. Fits of (311) reflections of XRD patterns of nano-maghemite samples irradiated with 155 MeV Xe ions with a fluence of 1×10^{14} ion cm^{-2} (**a**) and before irradiation (**b**).

Table 3. Crystallite size derived from the XRD of nano-maghemite samples, non-irradiated and irradiated with 155 MeV Xe ions with a fluence of 1×10^{14} ion cm^{-2}.

Sample	Linewidth (Degree) β	Crystallite Size (nm)		
		D_{min}	D	D_{max}
non-irradiated	1.26 ± 0.03	8.76	8.97	9.19
irradiated with a fluence of 1×10^{14} ion cm^{-2}	1.75 ± 0.18	5.85	6.46	7.20

An increased linewidth β, due to irradiation, could even be well seen by visual inspection in Figure 4.

Considering the results of the average crystallite size depicted in Table 3, we found that the non-irradiated and irradiated samples had different crystallite sizes. The average crystallite size of the non-irradiated sample was obtained to be around 9 ± 0.4 nm, while that of the irradiated sample resulted in an average crystallite size around 6.5 ± 0.7 nm. There was a significant decrease in the crystallite size upon the irradiation. The average

difference between the crystallite sizes of non-irradiated and irradiated samples was about 2.5 nm. Thus, we could distinguish the non-irradiated samples from the irradiated ones according to their crystallite size.

The results obtained with XRD also confirmed that both the non-irradiated and the irradiated samples contained nanosized maghemites. The obtained crystallite sizes were in the range where nano-maghemite showed superparamagnetic behavior at RT. This supported the results of the Mössbauer-spectroscopy characterization, which reflected the presence of superparamagnetism at RT. The decrease in crystallite size in the irradiated sample would require a higher extent of superparamagnetism at RT compared to the non-irradiated case, which was consistent with the Mössbauer results, thus confirming our interpretation. We can conclude that the change observed in the average crystallite size between the non-irradiated and swift heavy ion irradiated samples could support the Mössbauer results, and was consistent with the change in the RT superparamagnetism, due to an irradiation-induced decrease in the particle size. The Mössbauer and XRD results mutually supported and complemented each other.

Our results can be understood in terms of the interaction between the nano-maghemite and the swift heavy ions. In the interaction between matter and heavy ions, electron excitation and nuclear collision processes play the most significant role [63], in which, in our case, electron excitation processes dominated. These processes lead to the creation of a large number of crystal defects (primarily vacancies) in the irradiated sample [64]. The observed structural changes in the nano-maghemite could be mainly associated with the thermal spike mechanism [65–67]. The observed changes due to irradiation could be related to the accelerated diffusion of defects and ions via the molten tracks and ion beam mixing, similarly as reported in other works [43,68,69]. This theory also satisfactorily explained the results [49,50] obtained on other systems irradiated under the same irradiation conditions as the current one.

Defects created by irradiation are also capable of forming dislocations, as was already experienced in the case of high-energy heavy ion irradiations [39,50,70]. These dislocations can form grain boundaries under certain conditions. The formation of new grain boundaries, especially in the case of a nano-structured material with a small grain size, can lead to the fragmentation of the grains and the reduction of the effective grain size [71]. The more defects we created by irradiation, the more we reduced the grain size. The decrease in grain size resulted in a change in the superparamagnetic state, as a result of which the proportion of the superparamagnetic phase in the nano-structured material increased at a given temperature. This is what we observed with the help of Mössbauer spectroscopy and XRD in nano-maghemite as a result of swift Xe ion irradiation.

In our present case, the stopping power values, calculated using the SRIM-2013 code [72], for γ-Fe_2O_3 irradiated with 160 MeV and 155 MeV Xe ions were $(dE/dx)_e$ = 25.36 keV nm^{-1} and $(dE/dx)_e$ = 25.16 keV nm^{-1} for electron stopping and $(dE/dx)_n$ = 11.81 × 10^{-2} keV nm^{-1} and $(dE/dx)_n$ = 11.81 × 10^{-2} keV nm^{-1} for nuclear stopping, respectively. The penetration depths of these Xe ions in γ-Fe_2O_3 were 10.89 µm for 160 MeV energy and 10.70 µm for 155 MeV energy. In the case of the irradiation with 160 MeV energy with the lower fluence of 5 × 10^{13} ion cm^{-2} 28,464.9 vacancies per ion were created according to the SRIM code. The calculated $(dE/dx)_e$ = 25.36 keV nm^{-1} value of electronic stopping power could be found to be sufficient to produce enough thermal spikes for the observed transformation in the case of a fluence of 5 × 10^{13} ion cm^{-2}, when 1.42 × 10^{18} vacancies were generated in the nano-maghemite. In the case of 155 MeV Xe ion irradiation with the higher fluence of 1 × 10^{14} ion cm^{-2}, an even larger amount, 31 × 10^{18} vacancies, were created in the nano-maghemite, which could induce an even stronger effect, creating a much larger amount of irradiation-induced superparamagnetic region than in the case of the lower fluence irradiation. The results we obtained for the fluence threshold were consistent with those reported for different oxides [36,43,49,50,68,69,73,74] taking into account the difference in the irradiation parameters. The electron stopping power in our case far exceeded the 6 keV nm^{-1} threshold for dislocation formation estab-

lished by Khara et al. [39], who developed a computer model to estimate dislocation formations created by swift heavy ion irradiation, which strongly confirmed that we had a suitable amount of dislocations forming new grain boundaries resulting in increased amounts of superparamagnetic regions with fluence in nano-maghemite upon the irradiation.

4. Conclusions

Irradiation-induced changes upon swift heavy ion irradiation applying 160 MeV $^{132}Xe^{26+}$ ions with a fluence of 5×10^{13} ion cm^{-2} and 155 MeV $^{132}Xe^{26+}$ ions with a fluence of 1×10^{14} ion cm^{-2} were found in the superparamagnetic state of the nano-maghemite powder by the help of ^{57}Fe Mössbauer spectroscopy and XRD.

The Mössbauer spectra of the non-irradiated nano-maghemite samples showed typical relaxation spectra at room temperature according to their superparamagnetic state resulting from the particle size in the nano-range, which was found to be around 9 nm by XRD.

The room temperature Mössbauer spectra of irradiated nano-maghemites showed a fluence-dependent collapse of the relaxation spectrum reflecting an acceleration of the superparamagnetic relaxation process, which corresponded well to the significant decrease in the average particle size (to about 6.5 nm in the case of higher fluence) determined by XRD. In the case of irradiation with the fluence of 1×10^{14} ion cm^{-2}, the Mössbauer measurement indicated the appearance of the superparamagnetic phase even at 80 K, too.

The swift heavy ion irradiation-induced changes in the superparamagnetic state of maghemite could be interpreted in terms of the thermal spike model of the energy deposition of heavy ions involving irradiation-induced defect creation. The defects could be developed in the form of dislocations resulting in the formation of new grain boundaries, leading to the fragmentation of the grains and the reduction of the grain size of nano-maghemite. The decrease in grain size was manifested as change in the superparamagnetic state.

Author Contributions: Conceptualization, E.K., S.S. and J.P.; methodology, S.S., D.S., R.V. and B.H.; software, S.S.; validation, E.K., J.P., L.M. and Z.H.; formal analysis, E.K., S.S., L.M., M.K., B.H. and D.S.; investigation, E.K., S.S., L.K. (Lukáš Kouřil), D.S., R.V., Z.H., M.K., B.H., V.A.S. and S.K.; resources, J.P., L.M. and Z.H.; data curation, E.K., S.S. and B.H.; writing—original draft preparation, E.K. and S.S.; writing—review and editing, E.K., J.P., L.M., V.A.S., S.K., R.V., L.K. (Lukáš Kouřil) and Z.H.; visualization, S.S.; supervision, E.K. and J.P.; project administration, L.M. and L.K. (Luboš Krupa); funding acquisition, J.P., L.M. and Z.H., E.K. and L.K. (Luboš Krupa). All authors have read and agreed to the published version of the manuscript.

Funding: The research was supported by grants of the Hungarian National Research, Development and Innovation Office (OTKA projects No K43687, K68135, K100424, K115913, K115784) and by the Czech–Hungarian Intergovernmental Fund, Grant No. CZ-11/2007 (MEB040806). This work was also supported by the internal IGA grant of Palacký University (IGA_PrF_2024_002). The authors from Palacký University Olomouc want to thank the project CZ.02.1.01/0.0/0.0/17_049/0008408 of the Ministry of Education, Youth & Sports of the Czech Republic for their support as well.

Data Availability Statement: The raw data supporting the conclusions of this article will be made available by the authors on request.

Acknowledgments: We are grateful to Z. Klencsár (Centre for Energy Research, Budapest) for his participation in discussions.

Conflicts of Interest: The authors declare no conflict of interest.

References

1. Harish, V.; Tewari, D.; Gaur, M.; Yadav, A.B.; Swaroop, S.; Bechelany, M.; Barhoum, A. Review on Nanoparticles and Nanostructured Materials: Bioimaging, Biosensing, Drug Delivery, Tissue Engineering, Antimicrobial, and Agro-Food Applications. *Nanomaterials* **2022**, *12*, 457. [CrossRef] [PubMed]
2. Baig, N.; Kammakakam, I.; Falath, W. Nanomaterials: A review of synthesis methods, properties, recent progress, and challenges. *Mater. Adv.* **2021**, *2*, 1821–1871. [CrossRef]
3. Khan, I.; Saeed, K.; Khan, I. Nanoparticles: Properties, applications and toxicities. *Arab. J. Chem.* **2019**, *12*, 908–931. [CrossRef]

4. Ealias, A.M.; Saravanakumar, M.P. A review on the classification, characterisation, synthesis of nanoparticles and their application. *IOP Conf. Ser. Mater. Sci. Eng.* **2017**, *263*, 032019. [CrossRef]
5. Ali, A.; Shah, T.; Ullah, R.; Zhou, P.; Guo, M.; Ovais, M.; Tan, Z.; Rui, Y.K. Review on Recent Progress in Magnetic Nanoparticles: Synthesis, Characterization, and Diverse Applications. *Front. Chem.* **2021**, *9*, 629054. [CrossRef] [PubMed]
6. Joudeh, N.; Linke, D. Nanoparticle classification, physicochemical properties, characterization, and applications: A comprehensive review for biologists. *J. Nanobiotechnol.* **2022**, *20*, 262. [CrossRef]
7. Mitchell, M.J.; Billingsley, M.M.; Haley, R.M.; Wechsler, M.E.; Peppas, N.A.; Langer, R. Engineering precision nanoparticles for drug delivery. *Nat. Rev. Drug. Discov.* **2021**, *20*, 101–124. [CrossRef]
8. Samrot, A.V.; Ali, H.H.; Selvarani, J.; Faradjeva, A.E.; Prakash, R.P.; Suresh, P.; Kumar, S. Adsorption efficiency of chemically synthesized Superparamagnetic Iron Oxide Nanoparticles (SPIONs) on crystal violet dye. *Curr. Res. Green Sustain. Chem.* **2021**, *4*, 100066. [CrossRef]
9. Frantellizzi, V.; Conte, F.M.; Pontico, M.; Pani, A.; Pani, R.; De Vincentis, G. New Frontiers in Molecular Imaging with Superparamagnetic Iron Oxide Nanoparticles (SPIONs): Efficacy, Toxicity, and Future Applications. *Nucl. Med. Mol. Imaging* **2020**, *54*, 65–80. [CrossRef]
10. Nelson, N.R.; Port, J.D.; Pandey, M.K. Use of Superparamagnetic Iron Oxide Nanoparticles (SPIONs) via Multiple Imaging Modalities and Modifications to Reduce Cytotoxicity: An Educational Review. *J. Nanotheranostics* **2020**, *1*, 105–135. [CrossRef]
11. Wei, H.; Hu, Y.; Wang, J.; Gao, X.; Qian, X.; Tang, M. Superparamagnetic Iron Oxide Nanoparticles: Cytotoxicity, Metabolism, and Cellular Behavior in Biomedicine Applications. *Int. J. Nanomed.* **2021**, *16*, 6097–6113. [CrossRef]
12. Litewka, J.D.; Łazarczyk, A.; Hałubiec, P.; Szafrański, O.; Karnas, K.; Karewicz, A. Superparamagnetic Iron Oxide Nanoparticles—Current and Prospective Medical Applications. *Materials* **2019**, *12*, 617. [CrossRef]
13. Samrot, A.V.; Sahithya, C.S.; Selvarani, J.; Purayil, S.K.; Ponnaiah, P. A review on synthesis, characterization and potential biological applications of superparamagnetic iron oxide nanoparticles. *Curr. Res. Green Sustain. Chem.* **2021**, *4*, 100042. [CrossRef]
14. Sharma, V.; Singh, H.; Guleria, S.; Bhardwaj, M.; Puri, S.; Arya, S.K.; Khatri, M. Application of superparamagnetic iron oxide nanoparticles (SPIONs) for heavy metal adsorption: A 10-year meta-analysis. *Environ. Nanotechnol. Monit. Manag.* **2022**, *18*, 100716. [CrossRef]
15. Musielaka, M.; Piotrowskia, I.; Suchorska, W.M. Superparamagnetic iron oxide nanoparticles (SPIONs) as a multifunctional tool in various cancer therapies. *Rep. Pract. Oncol. Radiother.* **2019**, *24*, 307–314. [CrossRef]
16. Kandasamy, G.; Maity, D. Recent advances in superparamagnetic iron oxide nanoparticles (SPIONs) for in vitro and in vivo cancer nanotheranostics. *Int. J. Pharm.* **2015**, *496*, 191–218. [CrossRef]
17. Singh, F.; Mohapatra, S.; Stoquert, J.P.; Avasthi, D.K.; Pivin, J.C. Shape deformation of embedded metal nanoparticles by swift heavy ion irradiation. *Nucl. Instrum. Methods Phys. Res. Sect. B Beam Interact. Mater. At.* **2009**, *267*, 936–940. [CrossRef]
18. Dawi, E.A.; Vredenberg, A.M.; Rizza, G.; Toulemonde, M. Ion-induced elongation of gold nanoparticles in silica by irradiation with Ag and Cu swift heavy ions: Track radius and energy loss threshold. *Nanotechnology* **2011**, *22*, 215607. [CrossRef]
19. Sprouster, D.J.; Ridgway, M.C. Ion Beam Formation and Modification of Cobalt Nanoparticles. *Appl. Sci.* **2012**, *2*, 396–442. [CrossRef]
20. Rizza, G.; Attouchi, F.; Coulon, P.-E.; Perruchas, S.; Gacoin, T.; Monnet, I.; Largeau, L. Rayleigh-like instability in the ion-shaping of Au–Ag alloy nanoparticles embedded within a silica matrix. *Nanotechnology* **2011**, *22*, 175305. [CrossRef]
21. Giulian, R.; Kluth, P.; Araujo, L.L.; Sprouster, D.J.; Byrne, A.P.; Cookson, D.J.; Ridgway, M.C. Shape transformation of Pt nanoparticles induced by swift heavy-ion irradiation. *Phys. Rev. B* **2008**, *78*, 125413. [CrossRef]
22. Mishra, Y.K.; Kabiraj, D.; Avasthi, D.K.; Pivin, J.C. Swift heavy ion-induced dissolution of gold nanoparticles in silica matrix. *Radiat. Eff. Defects Solids* **2007**, *162*, 207–213. [CrossRef]
23. Avasthi, D.K.; Mishra, Y.K.; Singh, F.; Stoquert, J.P. Ion tracks in silica for engineering the embedded nanoparticles. *Nucl. Instrum. Methods Phys. Res. Sect. B Beam Interact. Mater. At.* **2010**, *268*, 3027–3034. [CrossRef]
24. Dufour, C.; Khomenkov, V.; Rizza, G.; Toulemonde, M. Ion-matter interaction: The three-dimensional version of the thermalspike model. Application to nanoparticle irradiation with swift heavy ions. *J. Phys. D Appl. Phys.* **2012**, *45*, 065302. [CrossRef]
25. Ridgway, M.C.; Giulian, R.; Sprouster, D.J.; Kluth, P.; Araujo, L.L.; Llewellyn, D.J.; Byrne, A.P.; Kremer, F.; Fichtner, P.F.P.; Rizza, G.; et al. Role of Thermodynamics in the Shape Transformation of Embedded Metal Nanoparticles Induced by Swift Heavy-Ion Irradiation. *Phys. Rev. Lett.* **2011**, *106*, 095505. [CrossRef]
26. Rizza, G.; Coulon, P.E.; Khomenkov, V.; Dufour, C.; Monnet, I.; Toulemonde, M.; Perruchas, S.; Gacoin, T.; Mailly, D.; Lafosse, X.; et al. Rational description of the ion-beam shaping mechanism. *Phys. Rev. B* **2012**, *86*, 035450. [CrossRef]
27. Krasheninnikov, A.V.; Nordlund, K. Ion and electron irradiation-induced effects in nanostructured materials. *J. Appl. Phys.* **2010**, *107*, 071301. [CrossRef]
28. Dawi, E.A.; Rizza, G.; Mink, M.P.; Vredenberg, A.M.; Habraken, F.H.P.M. Ion beam shaping of Au nanoparticles in silica: Particle size and concentration dependence. *J. Appl. Phys.* **2009**, *105*, 074305. [CrossRef]
29. Klaumünzer, S. Modification of nanostructures by high-energy ion beams. *Nucl. Instrum. Methods Phys. Res. Sect. B Beam Interact. Mater. At.* **2006**, *244*, 1–7. [CrossRef]
30. Ren, F.; Jiang, C.; Liu, C.; Wang, J. Controlling the Morphology of Ag Nanoclusters by Ion Implantation to Different Doses and Subsequent Annealing. *Phys. Rev. Lett.* **2006**, *97*, 165501. [CrossRef]

31. Zhang, Y.; Weber, W.J. Ion irradiation and modification: The role of coupled electronic and nuclear energy dissipation and subsequent nonequilibrium processes in materials. *Appl. Phys. Rev.* **2020**, *7*, 041307. [CrossRef]
32. Rizza, G.; Cheverry, H.; Gacoin, T.; Lamasson, A.; Henry, S. Ion beam irradiation of embedded nanoparticles: Toward an in situ control of size and spatial distribution. *J. Appl. Phys.* **2007**, *101*, 014321. [CrossRef]
33. Ren, F.; Cai, G.X.; Xiao, X.H.; Fan, L.X.; Liu, C.; Fu, D.J.; Wang, J.B.; Jiang, C.Z. Ion irradiation induced hollow and sandwiched nanoparticles. *J. Appl. Phys.* **2008**, *103*, 084308. [CrossRef]
34. Ren, F.; Jiang, C.Z.; Liu, C.; Wang, J.B. Fabrication and annihilation of nanovoids in Cu nanoclusters by ion implantation into silica and subsequent annealing. *Appl. Phys. Lett.* **2006**, *88*, 183114. [CrossRef]
35. Panda, R.; Khan, S.A.; Singh, U.P.; Naik, R.; Mishra, N.C. The impact of fluence dependent 120 MeV Ag swift heavy ion irradiation on the changes in structural, electronic, and optical properties of $AgInSe_2$ nano-crystalline thin films for optoelectronic applications. *RSC Adv.* **2021**, *11*, 26218–26227. [CrossRef]
36. Kumar, R.; Khan, M.W.; Srivastava, J.P.; Arora, S.K.; Sofin, R.G.S.; Choudhary, R.J.; Shvets, I.V. Swift heavy ion irradiation-induced modifications in structural, magnetic and electrical transport properties of epitaxial magnetite thin films. *J. Appl. Phys.* **2006**, *100*, 033703. [CrossRef]
37. Gokhale, S.; Lamba, S.; Kumari, N.; Singh, B.; Avasthi, D.K.; Kulkarni, S.K. Modifying the morphology and magnetic properties of magnetite nanoparticles using swift heavy ion irradiation. *Nucl. Instrum. Methods Phys. Res. Sect. B Beam Interact. Mater. At.* **2014**, *333*, 64–68. [CrossRef]
38. Bhat, R.; Dar, W.A. Effect of Swift Heavy Ion Irradiation on Iron Oxide Nanomaterials. *J. Pure Appl. Ind. Phys.* **2017**, *7*, 416–418. [CrossRef]
39. Khara, G.S.; Murphy, S.T.; Duffy, D.M. Dislocation loop formation by swift heavy ion irradiation of metals. *J. Phys. Condens. Matter* **2017**, *29*, 285303. [CrossRef]
40. Van Vuuren, A.J.; Skuratov, V.; O'Connell, J.; Saifulin, M.; Aralbayeva, G.; Dualetbekova, A.; Zdorovets, M. The Effect of Swift Heavy Ion Irradiation on the Microstructures of YAP, YAG and YIG. In *Interaction of Radiation with Solids, Proceedings of the 13th International Conference "Interaction of Radiation with Solids", Minsk, Belarus, 30 September–3 October 2019*; Uglov, V.V., Anishchik, V.M., Komarov, F.F., Maksimenko, S.A., Baran, L.V., Cherenda, N.N., Azarko, I.I., Eds.; Belarusian State University: Minsk, Belarus, 2019; pp. 123–125.
41. Khawal, H.A.; Dole, B.N. A study of the 160 MeV Ni^{7+} swift heavy ion irradiation effect of defect creation and shifting of the phonon modes on $Mn_xZn_{1-x}O$ thin films. *RSC Adv.* **2017**, *7*, 34736–34745. [CrossRef]
42. El Mendili, Y.; Bardeau, J.F.; Randrianantoandro, N.; Greneche, J.M.; Grasset, F. Structural behavior of laser-irradiated γ-Fe_2O_3 nanocrystals dispersed in porous silica matrix: γ-Fe_2O_3 to α-Fe_2O_3 phase transition and formation of ε-Fe_2O_3. *Sci. Technol. Adv. Mater.* **2016**, *17*, 597–609. [CrossRef]
43. Roller, T.; Bolse, W. Oxygen diffusion and oxide phase formation in iron under swift heavy ion irradiation. *Phys. Rev. B* **2007**, *75*, 054107. [CrossRef]
44. Rymzhanov, R.A.; Medvedev, N.; Volkov, A.E.; O'Connell, J.H.; Skuratov, V.A. Overlap of swift heavy ion tracks in Al_2O_3. *Nucl. Instrum. Methods Phys. Res. Sect. B Beam Interact. Mater. At.* **2018**, *435*, 121–125. [CrossRef]
45. Bolse, T.; Paulus, H.; Bolse, W. Swift heavy ion induced dewetting of metal oxide thin films on silicon. *Nucl. Instrum. Methods Phys. Res. Sect. B Beam Interact. Mater. At.* **2006**, *245*, 264–268. [CrossRef]
46. Joos, A.; Rümenapp, C.; Wagner, F.E.; Gleich, B. Characterisation of iron oxide nanoparticles by Mössbauer spectroscopy at ambient temperature. *J. Magn. Magn. Mater.* **2016**, *399*, 123–129. [CrossRef]
47. Wareppam, B.; Kuzmann, E.; Garg, V.K.; Singh, H. Mössbauer spectroscopic investigations on iron oxides and modified nanostructures: A review. *J. Mater. Res.* **2022**, *38*, 937–957. [CrossRef]
48. Mele, N.G.; Gamarra, D.I.; Zélis, P.M.; Sánchez, F.H.; Pasquevich, G.A. Evaluation of Nanoparticle-size distribution with Mössbauer Effect spectroscopy. *Hyperfine Interact.* **2022**, *243*, 18. [CrossRef]
49. Kuzmann, E.; Nomura, K.; Stichleutner, S.; Nakanishi, A.; Pechoušek, J.; Machala, L.; Homonnay, Z.; Vondrášek, R.; Skuratov, V.A.; Krupa, L.; et al. Swift heavy ion irradiation-induced amorphous iron and Fe–Si oxide phases in metallic ^{57}Fe layer vacuum deposited on surface of SiO_2/Si. *J. Mater. Res.* **2023**, *38*, 1061–1073. [CrossRef]
50. Kuzmann, E.; Stichleutner, S.; Machala, L.; Pechoušek, J.; Vondrášek, R.; Smrčka, D.; Kouřil, L.; Homonnay, Z.; Oshtrakh, M.I.; Mozzolai, A.; et al. Change in Magnetic Anisotropy at the Surface and in the Bulk of FINEMET Induced by Swift Heavy Ion Irradiation. *Nanomaterials* **2022**, *12*, 1962. [CrossRef]
51. Kobzi, B.; Watanabe, Y.; Akiyama, K.; Kuzmann, E.; Homonnay, Z.; Krehula, S.; Ristić, M.; Nishida, T.; Kubuki, S. ^{57}Fe-Mössbauer study and methylene blue decomposing effect of nanoparticle mixtures composed of metallic iron and maghemite. *J. Alloys Compd.* **2017**, *722*, 94–100. [CrossRef]
52. Klencsár, Z.; Kuzmann, E.; Vértes, A. User-Friendly Software for Mössbauer Spectrum Analysis. *J. Radioanal. Nucl. Chem.* **1996**, *210*, 105–118. [CrossRef]
53. Kündig, W.; Ando, K.J.; Constabaris, G.; Lindquist, R.H. Some Properties of Supported Small $\alpha-Fe_2O_3$ Particles Determined with the Mössbauer Effect. *Phys. Rev.* **1966**, *142*, 327. [CrossRef]
54. Murad, E.; Johnston, J.H. Iron Oxides and Oxyhydroxides. In *Mössbauer Spectroscopy Applied to Inorganic Chemistry*; Long, G.J., Ed.; Plenum Press: New York, NY, USA, 1987; Volume 2, pp. 507–582.

55. Kuzmann, E.; Nagy, S.; Vértes, A.; Weiszburg, T.; Garg, V.K. Geological and Mineralogical Applications of Mössbauer Spectroscopy. In *Nuclear Methods in Mineralogy and Geology*; Vértes, A., Nagy, S., Süvegh, K., Eds.; Plenum Press: New York, NY, USA, 1998; pp. 285–376.
56. Blume, M.; Tjon, J.A. Mössbauer Spectra in a Fluctuating Environment. *Phys. Rev.* **1968**, *165*, 446. [CrossRef]
57. Vértes, A.; Korecz, L.; Burger, K. *Mössbauer Spectroscopy*; Akadémiai Kiadó: Budapest, Hungary, 1979.
58. Stevens, J.G.; Stevens, V.E. *Mössbauer Effect Data Index*; Plenum Press: New York, NY, USA, 1968.
59. Coey, J.M.D.; Khalafalla, D. Superparamagnetic γ-Fe_2O_3. *Phys. Status Solidi (a)* **1972**, *11*, 229–241. [CrossRef]
60. Fardis, M.; Douvalis, A.P.; Tsitrouli, D.; Rabias, I.; Stamopoulos, D.; Kehagias, T.; Karakosta, E.; Diamantopoulos, G.; Bakas, T.; Papavassiliou, G. Structural, static and dynamic magnetic properties of dextran coated γ-Fe_2O_3 nanoparticles studied by ^{57}Fe NMR, Mössbauer, TEM and magnetization measurements. *J. Phys. Condens. Matter* **2012**, *24*, 156001. [CrossRef]
61. Schulz, D.; McCarthy, G. *See JCPDS Data No. 39-1346*; North Dakota State University: Fargo, ND, USA, 1987.
62. Scherrer, P. Bestimmung der Größe und der inneren Struktur von Kolloidteilchen mittels Röntgenstrahlen. *Göttinger Nachrichten Gesell.* **1918**, *2*, 98–100.
63. Was, G.S. *Fundamentals of Radiation Materials Science*, 2nd ed.; Springer: New York, NY, USA, 2017.
64. Seitz, F.; Koehler, J.S. Displacement of Atoms during Irradiation. In *Solid State Physics*; Seitz, F., Turnbull, D., Eds.; Academic Press: New York, NY, USA, 1956; Volume 2, pp. 305–448.
65. Klaumünzer, S. Thermal-Spike Models for Ion Track Physics: A Critical Examination. *Mat.-Fys. Meddelelser* **2006**, *52*, 293–328.
66. Toulemonde, M.; Paumier, E.; Dufour, C. Thermal spike model in the electronic stopping power regime. *Radiat. Eff. Defects Solids* **1993**, *126*, 201–206. [CrossRef]
67. Szenes, G. Thermal spike analysis of interface mixing induced by swift heavy ions. *Appl. Phys. Lett.* **2002**, *81*, 4622–4624. [CrossRef]
68. Yano, K.H.; Kohnert, A.A.; Dannya, B.; Edwards, J.; Holby, E.F.; Kaspar, T.C.; Kim, H.; Lach, T.G.; Taylor, S.D.; Wang, Y.; et al. Radiation-Enhanced Anion Transport in Hematite. *Chem. Mater.* **2021**, *33*, 2307–2318. [CrossRef]
69. Schattat, B.; Bolse, W. Fast heavy ion induced interface mixing in thin-film systems. *Nucl. Instrum. Methods Phys. Res. Sect. B Beam Interact. Mater. At.* **2004**, *225*, 105–110. [CrossRef]
70. Kuzmann, E.; Spirov, I.N. Mössbauer study of amorphous alloys irradiated with energetic heavy ions. *J. Nucl. Mater.* **1985**, *137*, 22–32. [CrossRef]
71. Pandian, M.; Krishnaprasanth, A.; Palanisamy, M.; Bangaru, G.; Meena, R.; Dong, C.-L.; Kandasami, A. Effects of Heavy Ion Irradiation on the Thermoelectric Properties of $In_2(Te_{1-x}Se_x)_3$ Thin Films. *Nanomaterials* **2022**, *12*, 3782. [CrossRef]
72. Ziegler, J.F.; Biersack, J.P.; Littmark, U. *The Stopping and Range of Ions in Solids*; Pergamon Press: New York, NY, USA, 1985.
73. Sapkota, P.; Aprahamian, A.; Chan, K.Y.; Frentz, B.; Macon, K.T.; Ptasinska, S.; Robertson, D.; Manukyan, K. Irradiation-induced reactions at the CeO_2/ SiO_2/Si interface. *J. Chem. Phys.* **2020**, *152*, 104704. [CrossRef]
74. Khalfaoui, N.; Stoquert, J.P.; Haas, F.; Traumann, C.; Meftah, A.; Toulemonde, M. Damage creation threshold of Al_2O_3 under swift heavy ion irradiation. *Nucl. Instrum. Methods Phys. Res. Sect. B Beam Interact. Mater. At.* **2012**, *286*, 247–253. [CrossRef]

Disclaimer/Publisher's Note: The statements, opinions and data contained in all publications are solely those of the individual author(s) and contributor(s) and not of MDPI and/or the editor(s). MDPI and/or the editor(s) disclaim responsibility for any injury to people or property resulting from any ideas, methods, instructions or products referred to in the content.